Received: 15 June 2019 | Revised: 16 October 2019 | Accepted: 24 October 2019

DOI: 10.1002/ddr.21623

RESEARCH ARTICLE

DDR WILEY

Synthesis, evaluation, molecular docking, and molecular dynamics studies of novel *N*-(4-[pyridin-2-yloxy]benzyl) arylamine derivatives as potential antitubercular agents

Ruchi Verma[1] | Helena I. M. Boshoff[2] | Kriti Arora[2] | Indira Bairy[3] | Mradul Tiwari[4] | Varadaraj Bhat G.[1] | G. Gautham Shenoy[1]

[1]Department of Pharmaceutical Chemistry, Manipal College of Pharmaceutical Sciences, Manipal Academy of Higher Education, Manipal, Karnataka, India

[2]Tuberculosis Research Section, Laboratory of Clinical Immunology and Microbiology, National Institute of Allergy and Infectious Diseases, National Institutes of Health, Bethesda, Maryland

[3]Department of Microbiology, Melaka Manipal Medical College, Manipal Academy of Higher Education, Manipal, Karnataka, India

[4]Department of Pharmaceutical Biotechnology, Manipal College of Pharmaceutical Sciences, Manipal Academy of Higher Education, Manipal, Karnataka, India

Correspondence
Dr. G. Gautham Shenoy, Professor, Department of Pharmaceutical Chemistry, Manipal College of Pharmaceutical Sciences, Manipal 576 104, Karnataka, India.
Email: gautham.gs@manipal.edu

Funding information
Department of Biotechnology

Abstract

A new series of novel triclosan (2,4,4′-trichloro-2′-hydroxydiphenylether) analogues were designed, synthesized, and screened for their in vitro antimycobacterial and antibacterial activities. Most of the compounds showed significant activity against *Mycobacterium tuberculosis* H37Rv strain with minimum inhibitory concentration (MIC) values in 20–40 μM range in GAST/Fe medium when compared with triclosan (43 μM) in the first week of assay, and after additional incubation, seven compounds, that is, **2a**, **2c**, **2g**, **2h**, **2i**, **2j**, and **2m**, exhibited MIC values at the concentration of 20–40 μM. The compounds also showed more significant activity against *Bacillus subtilis* and *Staphylococcus aureus*. The synthesized compounds showed druggable properties, and the predicted ADME (absorption, distribution, metabolism, and excretion) properties were within the acceptable limits. The *in silico* studies predicted better interactions of compounds with target protein residues and a higher dock score in comparison with triclosan. Molecular dynamics simulation study of the most active compound **2i** was performed in order to further explore the stability of the protein–ligand complex and the protein–ligand interaction in detail.

KEYWORDS
molecular dynamics, mycobacterial enoyl-reductase (InhA), pyridine, triclosan

1 | INTRODUCTION

According to the World Health Organization (WHO), tuberculosis (TB), a contagious disease mainly caused by *Mycobacterium tuberculosis* (MTb), is one of the oldest and biggest killers. As per WHO report, 2018, globally TB was responsible for death of 1.3 million HIV-negative and additional 0.3 million HIV-positive people. Emergence of multidrug resistant (MDR) TB and extensively drug resistant (XDR) TB has further complicated the scenario (Gandhi et al., 2006; WHO, 2018).

The current drug regimen for the drug susceptible (DS)-TB treatment involves a combination of isoniazid (INH), rifamycin, pyrazinamide, and ethambutol (Johnson et al., 2006), which can cure 95% of people suffering from DS-TB. MDR-TB needs longer treatment and involves treatment with second-line drugs, which are expensive, less effective, and less convenient with more adverse effects in comparison with the first-line drugs (Migliori, De Iaco, Besozzi, Centis, & Cirillo, 2007; Udwadia, Amale, Ajbani, & Rodrigues, 2012; Velayati et al., 2009). Global TB status presents an urgent need to develop safe and effective antitubercular drugs with alternate targets to avoid drug resistance.

The biosynthesis of the unique cell wall of *Mycobacterium* presents various drug targets providing significant potential for novel drug discovery (Barry, Crick, & McNeil, 2007). MTb utilizes the type II pathway fatty acid synthesis (FAS-II) pathway for extension of the fatty acid chains that are used for mycolic acid biosynthesis.

The FAS-II system is absent in higher eukaryotes and hence FAS-II enzymes are an attractive target as novel drugs with selective toxicity toward MTb could potentially be developed (Bloch, 1977). INH (pyridine derivative) inhibits the mycobacterial enoyl-reductase (InhA), but MDR and XDR MTb isolates have developed resistance toward INH primarily due to the KatG mutations. INH is a prodrug and is activated by the enzyme catalase peroxidase to form reactive species, which further reacts with NAD+ to form an INH-NAD adduct. This activated form of INH inhibits InhA, resulting in inhibition of mycolic acid biosynthesis and consequently mycobacterial cell death (Zhao et al., 2006). KatG encodes catalase peroxidase and is the prime reason for INH resistance. Mutation in *katG* activates INH and specifically the KatG variant, and S315T is found in about 94% of INH-resistant clinical isolates responsible for resistance (Nguyen, Claparols, Bernadou, & Meunier, 2001). Also mutation in the inhA (c-15t) promoter region results in inhA overexpression, thus resulting in the titration of the drug. Expression changes of the drug's activators, redox variation, inactivation of drug, and activation of efflux pump are the other mechanisms of INH resistance (Vilchèze & Jacobs, 2014). Inhibitors of the essential InhA component of the FAS-II system have been shown to have in vivo efficacy, and thus, there is precedence to support studies aimed at discovering InhA inhibitors (Levy et al., 1999; Nguyen et al., 2001; Rozwarski, Grant, Barton, Jacobs, & Sacchettini, 1998; Zhang, Heym, Allen, Young, & Cole, 1992; Zhao et al., 2006).

Triclosan (2,4,4′-trichloro-2′-hydroxydiphenyl ether) has been reported to inhibit InhA and thus inhibit fatty acid biosynthesis. Unlike INH, it directly inhibits InhA without further activation, but its role as an antitubercular agent is limited by its poor solubility (McLeod et al., 2001) and suboptimal bioavailability (Wang, Falany, & James, 2004). Despite these challenges, this small organic molecule provides a rational starting point for structure-based drug discovery to produce effective InhA inhibitors. Encouraged by the antitubercular activity of the 2-phenoxy-5-([arylamino]methyl)phenol derivatives synthesized by our research group, we decided to explore further these analogues by doing modification (Thomas et al., 2015). We synthesized novel pyridine ether derivatives with improved druggability, mimicking the structural features of triclosan, and assessed them for antitubercular activity. Since INH is an inhibitor of inhA, it was decided to introduce pyridine pharmacophore in the newly designed molecules, thus combining the features of triclosan and INH. Triclosan has two chlorine atoms in the structure, which contributes to higher lipophilicity. In order to reduce the lipophilicity of the molecules, the chlorine atoms were not retained. Furthermore, replacement of one of the phenyl rings with pyridine resulted in further reduction of lipophilicity of the molecules. Based on the literature data as well as the work carried out in our laboratory, a linker with two atoms was introduced between the aryl substituent and B-ring (Freundlich et al., 2009; Hartkoorn et al., 2012; Lu & Tonge, 2008).

Drug discovery process is time-consuming and very expensive. It involves contribution by experts from various disciplines. The success rate in drug discovery is extremely low. Out of the several thousands of molecules that are synthesized, only a few make into the clinical trials. Eliminating the unsuitable molecules in the early phase of drug discovery is essential to reduce the cost of drug discovery. Computational techniques are being used for the identification of lead molecules among the several thousands of molecules designed and their optimization. Advanced computational techniques have made lead identification and optimization process rapid (Taft, da Silva, & da Silva, 2008). These techniques help in identifying most promising molecules among several thousands of molecules that are initially designed. Ligand-based drug design (LBDD) and structure-based drug design (SBDD) are the two types of computer-aided dug design (CADD) approaches that are being used for drug design (Ece, 2019). Molecular docking study is an important study that helps to understand the nature of interaction between target residues and the designed molecule. The understanding of the nature of interactions helps in bringing about structural modifications and establish structure–activity relationship (Tahtaci, Karacık, Ece, Er, & Seker, 2018). Hence, supporting computational studies were carried out to explore the plausible interaction of the synthesized molecules with the target protein residue and to gather information related to the structural requirements of this scaffold to enhance their antitubercular potential. For this purpose, the published X-ray crystal structure of MTb InhA (pdb 3FNE) was used. This pdb consists of the crystal structure of InhA bound to a triclosan derivative. As most of the novel compounds have ADME (absorption, distribution, metabolism, and excretion) properties that remain to be experimentally validated, these properties and other drug-like properties were determined in silico for the synthesized compounds. Molecular dynamics (MD) studies give an insight into the protein dynamics, provide the possible binding sites, and also give clear information on the stable interaction over the simulation time period. The Desmond module of maestro was used for this purpose. Desmond can compute energies and forces for the standard fixed-charged force fields used in biomolecular simulations. Desmond supports algorithms normally used to perform fast and accurate MD. Long-range electrostatic energy and forces are calculated using particle-mesh-based Ewald techniques (Desmond, 2015). MD studies were performed for the most active compound and were compared with the triclosan.

2 | EXPERIMENTAL

2.1 | Material and methods

2.1.1 | Reagents and chemicals

All commercially available materials and solvents were used without any further purification. Media components for 7H9 and glycerol-alanine-salts-Tween-80 with iron (GAST-Fe) were purchased from Difco and Sigma, respectively. HepG2 and Vero cell lines used in this study were procured from the National Center for Cell Science, Pune, India, and maintained in high-glucose DMEM medium with 10% FBS and 1% antibiotic–antimycotic solution, at 37°C in a CO_2 incubator under 5% CO_2 (CLS-170-B-8, Serial No. 201020569, Esco Micro Pte. Ltd.). Column chromatography was performed for the isolation of the pure compounds from the crude reaction mixture on 100–200 mesh silica

gel purchased from Merck. All reactions were monitored, and purity of the compounds was checked by thin-layer chromatography (TLC, aluminum-coated sheets of silica gel 60F24, Merck, India). Melting points were determined with a laboratory melting point apparatus and are uncorrected. ^{1}H NMR and ^{13}C NMR spectra were recorded on a nuclear magnetic resonance (NMR) spectrometer (AV400—400 MHz, high-resolution multinuclear FT-NMR spectrometer, Bruker) in DMSO-d_6 (Dimethyl sulfoxide) as a solvent. Chemical shifts are reported here in parts per million (ppm). Mass spectrometric analysis was performed using LC–MS (linear ion trap, APCI mode, LC/MS, Thermo Fisher Scientific LTQ21532 series). δIR spectral data were recorded on an FT-IR spectrophotometer (IR Affinity-1, Shimadzu, Japan) in KBr pellets. The characteristic IR absorption frequencies are presented as wave numbers (cm^{-1}).

2.1.2 | Synthesis

*General procedure for the synthesis of 4-(pyridin-2-yloxy) benzaldehyde, **1***

Solution of 4-hydroxybenzaldehyde (2.0 mmol), 2-bromopyridine (0.95 g, 6.0 mmol), and potassium carbonate (0.87 g, 6.0 mmol) in dimethylacetamide (5 ml) were refluxed for 24 hr. The progress of the reaction was monitored by TLC using the hexane:ethyl acetate (8:2) solvent system. After reaction completion (24 hr), the reaction mixture was diluted using water (100 ml) by continuous stirring and the residue obtained was extracted using dichloromethane (3 × 50 ml). The combined organic layers were separated, dried over anhydrous $MgSO_4$, and evaporated under vacuum. The crude compound obtained was purified by column chromatography over silica 100–200 with hexane:ethyl acetate (8:2) as the mobile phase to afford 4-(pyridin-2-yloxy)benzaldehyde (Zheng et al., 2018).

Yield = 0.20 g (24%); mp = 35–36°C; R_f = 0.80 (hexane:ethyl acetate = 8:2); ^{1}H NMR (400 MHz, DMSO-d_6): δ 9.98 (s, 1H), 8.22 (s, 1H), 7.97–7.92 (m, 3H), 7.32 (d, *J* = 8.224 Hz, 2H), 7.32–7.24 (m, 1H), 7.16 (d, *J* = 7.6 Hz, 2H).

General procedure for the synthesis of N-*(4-(pyridin-2-yloxy)benzyl) arylamine **(2a–2m)***

To a solution of 4-(pyridin-2-yloxy)benzaldehyde (**1**) (0.2 g, 0.93 mmol) in methanol (10 ml), amine (1.12 mmol) was added and the mixture was refluxed until reaction completion. After the reaction was over, the reaction mixture was cooled and $NaBH_3CN$ (1.86 mmol) was added. The reaction mixture was refluxed. The progress of the reaction was monitored by TLC, using hexane:ethylacetate (8:2) as the mobile phase. When the reaction completed (8 hr), the solvent from the reaction mixture was evaporated under vacuum. Ice-cold water was added to the residue obtained and the product was extracted with ethyl acetate (3 × 25 ml). The combined organic layer was washed with water, dried using anhydrous $MgSO_4$, and evaporated using vacuum. The crude product obtained was purified using column chromatography over silica 100–200 with hexane:ethylacetate (9:1) as the mobile phase to get the target compound *N*-(4-(pyridin-2-yloxy)benzyl)arylamine (Thomas et al., 2015).

N-*(4-(pyridin-2-yloxy)benzyl)aniline **(2a)***

Yield = 0.50 g (72%); mp = 78–80°C; R_f = 0.80 (hexane:ethyl acetate = 8:2); IR (KBr, cm^{-1}) = 3,390.86, 3,047.53, 3,018.60, 1,465.90, 1,506.41, 1,595.13, 1,249.87, 1,197.79, 1,151.50; ^{1}H NMR (400 MHz, DMSO-d_6): δ 8.13 (s, 1H), 7.84 (d, *J* = 5.2 Hz, 1H), 7.39 (s, 2H), 7.06 (d, *J* = 4.4 Hz, 6H), 6.59–6.50 (m, 3H), 6.25 (d, *J* = 4.4 Hz, 1H), 4.26 (d, *J* = 8.0 Hz, 2H); ^{13}C NMR (100.62 MHz, DMSO-d_6): 163.61, 152.99, 149.11, 147.86, 140.56, 136.92, 129.32, 128.89, 121.53, 119.36, 116.24, 112.76, 111.86, 46.38; calculated for $C_{18}H_{16}N_2O$ [M+]: 276.34.43, found LC–MS (-APCI, *m/z*): 275.90 (M–H)$^-$.

4-Methoxy-N-*(4-(pyridin-2-yloxy)benzyl)aniline **(2b)***

Yield = 0.52 g (67.6%); mp = 52–54°C; R_f = 0.82 (hexane:ethyl acetate = 8:2); IR (KBr, cm^{-1}) =3,342.64, 3,057.17, 3,022.45, 2,997.38, 1,593.20, 1,512.19, 1,465.90, 1,253.73, 1,109; ^{1}H NMR (400 MHz, DMSO-d_6): δ 8.14 (t, *J* = 5.0, 1H), 7.85 (ddd, *J* = 8.8, 7.3, 2.0 Hz, 1H), 7.39 (d, *J* = 8.2 Hz, 2H), 7.16–7.03 (m, 3H), 7.01 (d, *J* = 8.3 Hz, 1H), 6.74–6.66 (m, 2H), 6.61–6.50 (m, 2H), 5.85 (t, *J* = 6.2 Hz, 1H), 4.22 (d, *J* = 6.1 Hz, 2H), 3.63 (s, 3H); ^{13}C NMR (100.62 MHz, DMSO-d_6): 163.61, 152.93, 151.19, 147.86, 143.33, 140.57, 137.19, 128.93, 121.48, 119.35, 115.05, 113.80, 111.85, 55.75, 47.18; calculated for $C_{19}H_{18}N_2O_2$ [M+]: 306.37, found LCMS (-APCI, *m/z*): 305.13 (M–H)$^-$.

3-*Methoxy*-N-*(4-(pyridin-2-yloxy)benzyl)aniline **(2c)***

Yield = 0.48 g (62.4%); mp = 48–50°C; R_f = 0.81 (hexane:ethyl acetate = 8:2); IR (KBr, cm^{-1}) =3,340, 3,089, 2,997, 1,608.63, 1,593.20, 1,247, 1,205, 1,163, 1,240.23; ^{1}H NMR (400 MHz, DMSO-d_6): 8.13 (t, *J* = 4.9 Hz, 1H), 7.84 (ddd, *J* = 8.8, 7.2, 2.0 Hz, 1H), 7.37 (d, *J* = 8.2 Hz, 2H), 7.15–7.03 (m, 3H), 7.00 (d, *J* = 8.3 Hz, 1H), 6.94 (t, *J* = 8.0 Hz, 1H), 6.28 (t, *J* = 6.1 Hz, 1H), 6.20 (dd, *J* = 8.1, 2.1 Hz, 1H), 6.16–6.07 (m, 2H), 4.24 (d, *J* = 6.1 Hz, 2H), 3.64 (s, 3H); ^{13}C NMR (100.62 MHz, DMSO-d_6): 163.61, 160.75, 152.97, 150.44, 147.86, 140.58, 136.93, 130.01, 128.88, 121.54, 119.36, 111.86, 105.93, 101.67, 98.59, 55.05, 46.37; calculated for $C_{19}H_{18}N_2O_2$ [M+]: 306.37, found LC–MS (-APCI, *m/z*): 305.26 (M–H)$^-$.

4-Methyl-N-*(4-(pyridin-2-yloxy)benzyl)aniline **(2d)***

Yield = 0.569 g (73.9%); mp = 56–58°C; R_f = 0.84 (hexane:ethyl acetate = 8:2); IR (KBr, cm^{-1}) =3,390.86, 3,053.32, 3,024.38, 1,583.56, 1,516.05, 1,465.90, 1,246.02, 1,201.65, 1,153.43; ^{1}H NMR (400 MHz, DMSO-d_6): δ 8.14 (t, *J* = 5.0 Hz, 1H), 7.84 (ddd, *J* = 8.3, 7.2, 2.0 Hz, 1H), 7.38 (d, *J* = 8.3 Hz, 2H), 7.16–7.03 (m, 3H), 7.01 (dt, *J* = 8.3, 0.9 Hz, 1H), 6.87 (d, *J* = 8.0 Hz, 2H), 6.55–6.48 (m, 2H), 6.05 (t, *J* = 6.2 Hz, 1H), 4.24 (d, *J* = 6.1 Hz, 2H), 2.14 (s, 3H); ^{13}C NMR (100.62 MHz, DMSO-d_6): 163.61, 152.92, 147.85, 146.82, 140.56, 137.11, 129.76, 128.86, 124.57, 121.49, 119.34, 112.90, 111.84, 46.61, 20.54; calculated for $C_{19}H_{18}N_2O$ [M+]: 290.37, found LC–MS (-APCI, *m/z*): 289.13 (M–H)$^-$.

3-*Methyl*-N-*(4-(pyridin-2-yloxy)benzyl)aniline **(2e)***

Yield = 0.50 g (68.6%); mp = 55–57°C; R_f = 0.82 (hexane:ethyl acetate = 8:2); IR (KBr, cm^{-1}) = 3,344.57, 3,041.74, 2,927.94, 1,597.06,

1,512.19, 1,469.76, 1,421.54, 1,274.95, 1,201.65, 1,159.22; ^{1}H NMR (400 MHz, DMSO-d_6): δ 8.13 (d, *J* = 4.6 Hz, 1H), 7.87–7.78 (m, 1H), 7.37 (dd, *J* = 8.4, 2.0 Hz, 2H), 7.14–6.87 (m, 5H), 6.43 (s, 1H), 6.36 (dd, *J* = 18.6, 7.8 Hz, 2H), 6.13 (t, *J* = 6.1 Hz, 1H), 4.24 (d, *J* = 6.0 Hz, 2H), 2.15 (d, *J* = 2.0 Hz, 3H); ^{13}C NMR (100.62 MHz, DMSO-d_6): 163.61, 152.95, 149.12, 147.86, 140.57, 138.23, 137.04, 129.20, 128.86, 121.51, 119.35, 117.21, 113.46, 111.85, 109.96, 46.34, 21.86; calculated for $C_{19}H_{18}N_2O$ [M+]: 290.37, found LC–MS (-APCI, *m/z*): 289.12 $(M-H)^-$.

2-Methyl-N-*(4-(pyridin-2-yloxy)benzyl)aniline* ***(2f)***

Yield = 0.52 g (71.3%); mp = 51–53°C; R_f = 0.81 (hexane:ethyl acetate = 8:2); IR (KBr, cm^{-1}) =3,340.71, 3,014.74, 2,951.09, 1,595.13, 1,510.26, 1,495.90, 1,274.95, 1,201.65, 1,153.43; ^{1}H NMR (400 MHz, DMSO-d_6): δ 8.13 (dd, *J* = 5.0, 2.0 Hz, 1H), 7.87–7.78 (m, 1H), 7.45–7.35 (m, 2H), 7.16–7.01 (m, 3H), 7.03–6.87 (m, 3H), 6.52–6.38 (m, 2H), 5.63 (t, *J* = 6.1 Hz, 1H), 4.35 (d, *J* = 6.0 Hz, 2H), 2.16 (s, 3H); ^{13}C NMR (100.62 MHz, DMSO-d_6): 163.61, 152.88, 147.85, 146.57, 140.56, 137.13, 130.21, 128.59, 127.08, 122.24, 121.50, 119.34, 116.18, 111.85, 110.02, 46.28, 18.25; calculated for $C_{19}H_{18}N_2O$ [M+]: 290.37, found LC–MS (-APCI, *m/z*): 289.10 $(M-H)^-$.

4-Chloro-N-*(4-(pyridin-2-yloxy)benzyl)aniline* ***(2g)***

Yield = 0.55 g (70%); mp = 94–96°C; R_f = 0.87 (hexane:ethyl acetate = 8:2); IR (KBr, cm^{-1}) = 3,321, 3,059.10, 3,024.38, 1,597.06, 1,510.26, 1,465.90, 1,273.02, 1,207.44, 1,151.50; ^{1}H NMR (400 MHz, DMSO-d_6): δ 8.14 (dd, *J* = 4.9, 2.0 Hz, 1H), 7.85 (ddd, *J* = 8.8, 7.3, 2.1 Hz, 1H), 7.42–7.33 (m, 2H), 7.25–7.02 (m, 5H), 7.02 (d, *J* = 8.2 Hz, 1H), 6.65–6.56 (m, 2H), 6.49 (t, *J* = 6.1 Hz, 1H), 4.26 (d, *J* = 6.0 Hz, 2H); ^{13}C NMR (100.62 MHz, DMSO-d_6): 163.58, 153.07, 147.99, 147.94, 140.58, 136.41, 130.86, 129.03, 128.91, 121.59, 119.20, 114.09, 111.87, 46.34; calculated for $C_{18}H_{15}ClN_2O$ [M+]: 310.78, found LC–MS (-APCI, *m/z*): 309.06 $(M-H)^-$.

3-Chloro-N-*(4-(pyridin-2-yloxy)benzyl)aniline* ***(2h)***

Yield = 0.489 g (63%); mp = 88–90°C; R_f = 0.85 (hexane:ethyl acetate = 8:2); IR (KBr, cm^{-1}) =3,323.35, 3,061.03, 3,022.45, 1,589.34, 1,508.33, 1,477.47, 1,276.88, 1,203.58, 1,153.43; ^{1}H NMR (400 MHz, DMSO-d_6): δ 8.17–8.10 (m, 1H), 7.88–7.79 (m, 1H), 7.41–7.34 (m, 2H), 7.15–7.00 (m, 4H), 7.04–6.97 (m, 1H), 6.65–6.57 (m, 2H), 6.54 (ddd, *J* = 13.6, 7.9, 2.1 Hz, 2H), 4.27 (d, *J* = 6.0 Hz, 2H); ^{13}C NMR (100.62 MHz, DMSO-d_6): 163.57, 153.11, 150.60, 147.86, 140.59, 136.24, 134.06, 130.84, 128.93, 121.63, 119.39, 115.62, 111.89, 111.87, 111.42, 46.10; calculated for $C_{18}H_{15}ClN_2O$ [M+]: 310.78, found LC–MS (-APCI, *m/z*): 309.17 $(M-H)^-$.

2-Chloro-N-*(4-(pyridin-2-yloxy)benzyl)aniline* ***(2i)***

Yield = 0.531 g (68%); mp = 86–88°C; R_f = 0.84 (hexane:ethyl acetate = 8:2); IR (KBr, cm^{-1}) = 3,419.79, 3,064.89, 3,016.67, 1,591.27, 1,508.33, 1,463.97, 1,274.95, 1,197.79, 1,153.43; ^{1}H NMR (400 MHz, DMSO-d_6): δ 8.13 (dd, *J* = 5.0, 2.0 Hz, 1H), 7.83 (t, *J* = 7.7 Hz, 1H), 7.41–7.34 (m, 2H), 7.25 (dd, *J* = 7.8, 1.4 Hz, 1H), 7.07 (qd, *J* = 11.0, 9.7, 6.5 Hz, 4H), 7.00 (d, *J* = 8.2 Hz, 1H), 6.64–6.51 (m, 2H), 6.14 (t, *J* = 6.3 Hz, 1H), 4.41 (d, *J* = 6.2 Hz, 2H); ^{13}C NMR (100.62 MHz, DMSO-d_6): 163.56, 153.04, 147.85, 144.32, 140.58, 136.37, 129.47, 128.57, 128.36, 121.60, 119.38, 118.31, 116.97, 112.10, 111.89, 45.88; calculated for $C_{18}H_{15}ClN_2O$ [M+]: 310.78, found LC–MS (-APCI, *m/z*): 309.68 $(M-H)^-$.

4-Fluoro-N-*(4-(pyridin-2-yloxy)benzyl)aniline* ***(2j)***

Yield = 0.60 g (81.0%); mp = 75–77°C; R_f = 0.79 (hexane:ethyl acetate = 8:2); IR (KBr, cm^{-1}) = 3,315.63, 3,089.96, 3,057.17, 3,030.17, 1,597.061512.19, 1,274.95, 1,207.44, 1,151.50; ^{1}H NMR (400 MHz, DMSO-d_6): δ 8.13 (t, *J* = 4.9 Hz, 1H), 7.89–7.79 (m, 1H), 7.42–7.34 (m, 2H), 7.16–6.96 (m, 4H), 6.95–6.84 (m, 2H), 6.63–6.53 (m, 2H), 6.20 (t, *J* = 5.6 Hz, 1H), 4.23 (d, *J* = 5.1 Hz, 2H); ^{13}C NMR (100.62 MHz, DMSO-d_6): 163.59, 155.89, 153.02, 147.85, 145.80, 140.59, 136.71, 128.95, 121.55, 119.37, 115.80, 115.58, 113.48, 113.40, 111.87, 46.88; calculated for $C_{18}H_{15}CFN_2O$ [M+]: 294.33, found LC–MS (-APCI, *m/z*): 293.30 $(M-H)^-$.

2-Fluoro-N-*(4-(pyridin-2-yloxy)benzyl)aniline* ***(2k)***

Yield = 0.57 g (77.0%); mp = 68–70°C; R_f = 0.77 (hexane:ethyl acetate = 8:2); IR (KBr, cm^{-1}) = 3,323.35, 2,881.65, 2,843.07, 1,606.70, 1,583.56, 1,274.95, 1,195.87,1,155.36; ^{1}H NMR (400 MHz, DMSO-d_6): 8.13 (t, *J* = 4.9 Hz, 1H), 7.83 (t, *J* = 8.3 Hz, 1H), 7.43–7.36 (m, 2H), 7.14–6.96 (m, 5H), 6.89 (t, *J* = 7.8 Hz, 1H), 6.62 (m, 3H), 4.35 (d, *J* = 6.3 Hz, 2H); ^{13}C NMR (100.62 MHz, DMSO-d_6): δ 163.57, 153.01, 150.20, 147.85, 140.58, 136.63, 128.68, 125.10, 121.54, 119.37, 115.98, 115.92, 114.69,112.68, 111.88, 45.77; calculated for $C_{18}H_{15}CFN_2O$ [M+]: 294.33, found LC–MS (-APCI, *m/z*): 293.09 $(M-H)^-$.

4-Bromo-N-*(4-(pyridin-2-yloxy)benzyl)aniline* ***(2l)***

Yield = 0.65 g (73%); mp = 96–98°C; R_f = 0.79 (hexane:ethyl acetate = 8:2); IR (KBr, cm^{-1}) = 3,321.42, 3,059.10, 3,022.45, 1,595.13, 1,510, 1,465.90, 1,273.02, 1,205.51, 1,151.50; ^{1}H NMR (400 MHz, DMSO-d_6): δ 8.14 (dd, *J* = 5.0, 1.9 Hz, 1H), 7.85 (ddd, *J* = 8.6, 7.3, 2.0 Hz, 1H), 7.41–7.34 (m, 2H), 7.24–7.15 (m, 2H), 7.18–7.04 (m, 3H), 7.02 (d, *J* = 8.3 Hz, 1H), 6.61–6.48 (m, 3H), 4.26 (d, *J* = 6.0 Hz, 2H); ^{13}C NMR (100.62 MHz, DMSO-d_6): 163.58, 153.07, 148.34, 147.86, 140.59, 136.36, 131.83, 128.89, 121.60, 119.39, 114.68, 111.88, 106.84, 46.23; calculated for $C_{18}H_{15}BrN_2O$ [M+]: 355.24 found LC–MS (-APCI, *m/z*): 354.32 $(M-H)^-$.

3-bromo-N-*(4-(pyridin-2-yloxy)benzyl)aniline* ***(2m)***

Yield = 0.63 g (70.6%); mp = 92–94°C; R_f = 0.78 (hexane:ethyl acetate = 8:2); IR (KBr, cm^{-1}) = 3,325.28, 3,059.10, 3,020.53, 1,587.42, 1,506.41, 1,473.62, 1,246.02, 1,205.51, 1,153.43; ^{1}H NMR (400 MHz, DMSO-d_6): δ 8.13 (ddd, *J* = 5.0, 2.1, 0.9 Hz, 1H), 7.84 (ddd, *J* = 8.2, 7.2, 2.0 Hz, 1H), 7.41–7.28 (m, 2H), 7.21–7.05 (m, 3H), 7.09–6.95 (m, 2H), 6.76 (t, *J* = 2.1 Hz, 1H), 6.65 (ddd, *J* = 7.9, 1.9, 0.9 Hz, 1H), 6.63–6.55 (m, 2H), 4.27 (d, *J* = 6.0 Hz, 2H); ^{13}C NMR (100.62 MHz, DMSO-d_6): 163.57, 153.12, 150.78, 147.86, 140.59, 136.22, 131.18, 128.93, 122.79, 121.63, 119.39, 118.51, 114.82, 111.89, 111.68,

46.08; calculated for $C_{18}H_{15}BrN_2O$ [M+]: 355.24 found LC–MS (-APCI, *m/z*): 354.07 $(M-H)^-$.

2.1.3 | Biological activities

Antitubercular activity

All the synthesized compounds were assayed by microtiter dilution assay in a 96-well plate protocol using two different media, that is, regular 7H9-based medium and GAST-Fe (pH 6.6) medium for minimum inhibitory concentration (MIC) determination against MTb H37Rv. The MTb inoculum at approximately 2×10^5 CFU/well was used for this assay. Sterile stock solution of synthesized compounds and standard compounds was prepared in DMSO. The assay was performed using the serial dilution technique where the MTb inoculum was added to the assay plate containing serial twofold dilutions of the compounds in the medium of choice attaining a final cell concentration of 1×10^5 cfu/ml and the final compound concentration series range of 100 to 0.048 μM. INH and triclosan were taken as positive control. Plates were sealed in a ziplock bag and incubated at 37°C for 14 days. Plates were read after completion of Weeks 1 and 2 using inverted enlarging mirror plate reader and graded for growth and no growth. The MIC was defined as the lowest drug concentration that prevented growth of bacteria (Barot et al., 2014; Kaniga et al., 2016; Soares de Melo et al., 2015).

Antibacterial activity

All the synthesized compounds were tested for antibacterial activity by resazurin-based microtiter dilution assay in 96-well plates in the concentration range of 50 to 1.56 μg/ml. Four bacterial species were used, that is, *Bacillus subtilis*, *Pseudomonas aeruginosa*, *Staphylococcus aureus*, and *Escherichia coli*. At first, 100 μl of the test compound in 10% (v/v) DMSO was added to the first row of the microtiter plate and 50 μl of the nutrient broth was added to the remaining rows. The compounds were serially diluted using a multichannel pipette. Then, 10 μl of resazurin dye and 30 μl of 3.3× strength broth were added to each well to achieve the concentration of single strength. Finally, 10 μl of bacterial suspension (5×10^6 cfu/ml) was added to each well. The plates were sealed in a ziplock bag and placed in the incubator at 37°C for 18–24 hr. Ciprofloxacin and triclosan were used as positive controls. After 24 hr, any color change from violet to pink was recorded as positive. The lowest concentration where color change occurred was considered as the activity of the compound (Sharma, Kothapalli, Dongen, & Swaminathan, 2012).

Cytotoxicity

The cytotoxicity of the synthesized compounds was assessed using the MTT [3-(4, 5-dimethylthiazo-2-yl)-2,5-diphenyl-tetrazolium bromide] assay on Vero cells (from the kidneys of African Green monkey) and HepG2 cells (human liver cancer cell lines). This is a colorimetric assay involving the reduction of MTT to insoluble formazan by cellular enzymes (Guo et al., 2010). The test samples were prepared in various concentrations using DMEM and added to the 96-well plates. DMSO concentration was maintained at ≤0.1%. Then, 100 μl of sample dilutions were added to each well of 96-well plate containing Vero cells (10^4 cells/well) and incubated at 37°C for 72 hr. Inoculum was kept as positive control and media as negative control. After 72 hr of incubation, to each well, 50 μl of MTT was added and the plate was again incubated for 4 hr at 37°C. After 4 hr, 50 μl of sterile DMSO was added to dissolve any formazan crystals that had formed. Furthermore, the absorbance was recorded by using an ELISA plate reader at 540 nm, and the CC_{50} value was determined using the curve-fitting program (Ammerman, Beier-Sexton, & Azad, 2008; Guo et al., 2010).

As antitubercular drugs are associated with hepatotoxicity (Ajay et al., 2010), in vitro cell line studies were performed using MTT assay in HepG2 cells to assess the hepatotoxicity of the synthesized compounds. The protocol used was the same as that for Vero cell lines. Here, the concentration of HepG2 cells was kept as 5×10^3 cells/well and incubated for 24 hr before the addition of MTT. The following equations were used to calculate the percentage cell viability and percentage cell inhibition:

% Cell viability = (optical density of the test/optical density of control)/100% cell inhibition = 100−% cell viability.

2.1.4 | In silico studies

Molecular modeling

Molecular docking was performed to understand the binding mode of the compounds. The crystal structure of InhA complexed with triclosan derivative (PDB 3FNE) was downloaded from the Protein Data Bank. The protein preparation wizard module of Schrodinger 2017-4 was used to process the protein. The multistep process involved bond order assignment, hydrogens addition, treatment of disulfides, removal of unimportant water molecules within 5 Å of the binding site, hydrogen bond assignment via exhaustive sampling, and energy minimization to root mean square deviation (RMSD) 0.30 Å by OPLS-2003. A grid was generated at the center of the cocrystallized ligand (triclosan derivative) to include the cofactor and substrate-binding sites by utilizing default parameters of the software. The ligand was excluded from the protein and was limited to the enclosing box at the centroid. The docking procedure was validated by removing the cocrystallized ligand from the binding site and redocking it at the same binding site. The obtained RMSD score was 0.4163 Å. A 2D sketch tool of Schrodinger 2017-4 was used to draw the designed molecules, and the possible conformers (through Epik) were generated using the LigPrep module. Optimized potential for liquid simulation (OPLS) force field was used to obtain low-energy conformers of the designed molecules. Then single low-energy 3D conformers were docked using a flexible docking method with the catalytic site of the receptor using the extra precision (XP) Glide algorithm of Schrodinger suite 2017-4 (Bari & Haswani, 2017; Friesner et al., 2006; Harder et al., 2015; Malikanti et al., 2017; Schrödinger Release 2017-4, 2017; Sharma et al., 2018).

MD simulations

Protein dynamics changes during docking and with the help of MD simulation study, and the affinity of a molecule on various conformations of the target receptor can be measured. Hence, we performed

MD study using the Desmond module from Schrodinger (Desmond, 2015). MD simulations were carried out using Maestro version 11.4 (Schrodinger Inc.) on a HP computer with a Linux Ubuntu 18.04.1 LTS platform, Intel Haswell graphics card, 8 GB RAM, and Intel Core i3-4160 processor. First, a system builder panel was used for preparing the orthorhombic simulation box using an SPC explicit water model. The minimum distance between the protein surface and the solvent surface was 10 Å, and the charge was neutralized by adding sodium and chloride ions. The simulation was run for 20 ns, using NPT ensemble at a temperature of 300 K and atmospheric pressure (1.013 bar) using default setting before simulation. During MD simulation, the trajectory was written with 1,000 frames and a frame was captured at every 15 ps. Postmolecular dynamics analysis was performed using a simulation interaction diagram tool of the Schrodinger software.

In silico drug-likeliness and ADME prediction

The drug-like properties of the synthesized compounds were calculated using the QikProp module (v 5.4, Schrodinger release 2017-4). The properties such as molecular weight, hydrogen bond donor, hydrogen bond acceptor, log *p*, QPlog S, QPPCaco, QPlogBB, QPPMDCK, Percent Human Oral Absorption, CNS activity, and QPlogKhsa (Lipinski, Lombardo, Dominy, & Feeney, 1997; Sharma et al., 2012; Veber et al., 2002) were predicted using the QikProp module.

3 | RESULTS AND DISCUSSION

3.1 | Synthesis and spectral analysis

The final compounds were prepared as per the steps described in Scheme 1. 4-Hydroxy benzaldehyde was condensed with 2-bromopyridine to obtain 4-(pyridin-2-yloxy)benzaldehyde (Zheng et al., 2018). The aldehyde obtained (compound **1**) was reacted with various aromatic amines to obtain the target compounds **2a**–**2m** (Thomas et al., 2015). The mechanistic approach for the compounds (**2a**–**2m**) formation involves attack of nucleophilic amines on the electrophilic carbon atoms of aldehyde resulting in replacement of C=O bond with C=N bond, which is an imine or Schiff's base (Schiff base, 2014). Furthermore, the C=N bond was reduced with sodium cyanoborohydride to get the final compounds. The products were obtained in moderate yield (62–82%). The molecular characterization through NMR, IR, and mass spectroscopy confirmed their formation. The IR spectra of compounds **2a**–**2m** showed NH peak between 3,300 and 3,000 cm^{-1}. The 1H NMR spectra of the compound **2a**–**2m** exhibited aromatic protons in between 6.00 and 8.00 ppm and a doublet around 4.00 ppm representing two protons of NH—CH_2 group, thus confirming the formation of reduced Schiff bases (Additional spectral details are given in supplementary file).

3.2 | Antitubercular activity

All the synthesized compounds were evaluated for their antitubercular activity in vitro against MTb H37Rv (ATCC-27294) using the standard microbroth dilution minimum inhibitory concentration (MIC) protocol in two different media; regular 7H9-based medium; and GAST-Fe (pH 6.6) medium. The compounds were screened at 12 different concentrations, ranging from 100 to 0.048 μM. The results of in vitro antitubercular activity are presented in Table 1.

With GAST-Fe medium for minimum inhibitory concentration, compounds tested (series **2a**–**2m**) showed potent MIC values. All 13 compounds showed better or comparable activity with respect to triclosan, and among them, 5 compounds showed MIC ranging from 19 to 25 μM. The most potent compound was found to be 4-fluoro-substituted derivative with an MIC of 19 μM. After additional incubation (second week), except for the compound **2k** (MIC 70 μM), all the compounds exhibited activity equal to or better than triclosan, suggesting that the compounds maintained their ability to inhibit mycobacterial growth over time. The substantial activity of compounds after additional incubation suggests that the compounds maintained their ability to inhibit mycobacterial growth over time.

In 7H9-based medium, among the compounds tested (series **2a**–**2m**), compounds **2b**, **2f**, **2g**, and **2l** showed moderate MIC values of 41 μM, 40 μM, 40 μM, and 35 μM at the end of Week 1, but none of the compounds showed antitubercular activity better than triclosan (MIC 22 μM). At the end of Week 2, none of the compounds were found to display activity better than triclosan (MIC 43 μM). The lower MIC in GAST-Fe medium as compared to regular 7H9-based medium is likely driven by protein binding of the compounds to the BSA component of 7H9-based broth.

3.3 | Antibacterial activity

The synthesized compounds were screened against *P. aeruginosa*, *S. aureus*, *E. coli*, and *B. subtilis* for antibacterial activity. The

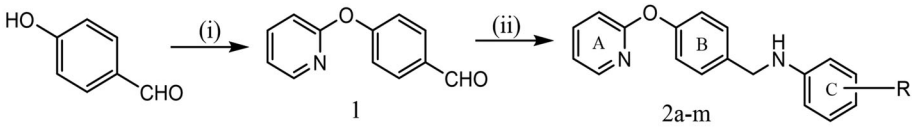

R= 2a. H, 2b. 4-OCH_3, 2c. 3-OCH_3, 2d. 4-CH_3, 2e. 3-CH_3, 2f. 2-CH_3, 2g. 4-Cl, 2h. 3-Cl, 2i. 2-Cl, 2j. 4-F, 2k. 2-F, 2l. 4-Br, 2m. 3-Br

Reagents and conditions: (i) C_5H_4BrN, K_2CO_3, $CH_3CN(CH_3)_2$, 156°C-160°C, 24h; (ii) $ArNH_2$, $NaBH_3CN$, CH_3OH, Gla.AcOH, 60-70°C,12h.

SCHEME 1 Synthesis of N-(4-(pyridin-2-yloxy)benzyl) arylamine derivatives

TABLE 1 In vitro antimycobacterial activity and cytotoxicity of compounds **(2a–2m)**

Compounds	MIC[a] (μM) (GAST/Fe)		MIC (μM) (7H9/ADC/Tween)		CC_{50}[b] (μM)	
	Week 1	Week 2	Week 1	Week 2	[c]Vero	[d]HepG2
2a	25	37	>50	>50	>300	>300
2b	41	41	41	82	>300	>300
2c	25	37	>50	>50	>300	>300
2d	22	43	86	86	>300	>300
2e	43	43	>100	>100	>300	>300
2f	43	43	>100	>100	>300	>300
2g	40	40	40	80	>300	>300
2h	20	40	40	80	>300	>300
2i	20	20	>100	>100	>300	>300
2j	19	25	>50	>50	>300	>300
2k	43	43	>100	>100	>300	>300
2l	35	70	70	70	>300	>300
2m	35	35	35	70	>300	>300
Triclosan	43	43	22	43	>300	>300
Isoniazid	0.2	0.2–0.4	0.78	1.5	–	–

[a]MIC is defined as the minimal drug concentration required to stop the growth of *Mycobacterium tuberculosis* H37Rv.
[b]CC_{50} is defined as the minimal drug concentration required for 50% death of viable cells.
[c]Vero: African green monkey kidney cell line.
[d]HepG2: human liver cells.

TABLE 2 In vitro antibacterial activity of compounds **2a–2m**

Compounds	*Bacillus subtilis* activity (μg/ml)	*Pseudomonas aeruginosa* activity (μg/ml)	*Staphylococcus aureus* activity (μg/ml)	*Escherichia coli* activity (μg/ml)
2a	1.6	>25	1.8	>25
2b	>6.24	>25	>3.1	>25
2c	1.6	>25	1.6	>50
2d	1.8	>50	1.8	>25
2e	>3.1	>25	>6.2	>50
2f	1.8	>50	1.6	>25
2g	>6.2	>25	>3.1	>50
2h	1.8	>50	1.8	>25
2i	1.8	>25	1.6	>25
2j	1.6	>12.5	1.8	>12.5
2k	1.8	>25	1.6	>25
2l	>3.1	>25	>6.2	>25
2m	>6.2	>50	>3.1	>50
Triclosan	1.8	>25	1.8	>3.2
Ciprofloxacin	1.6	1.6	1.6	1.6

preliminary screening of the compounds was conducted at concentrations ranging from 50 to 1.56 μg/ml. The results are displayed in Table 2. The compounds were found to be more active against *B. subtilis* and *S. aureus* than those against *P. aeruginosa* and *E. coli*. The results suggest that the compounds are mostly active against gram-positive bacteria.

3.4 | In vitro cytotoxicity evaluation

The compounds were found to be safe when screened against normal Vero cell lines as all the compounds showed activity >300 μM in cell viability assay. The synthesized compounds were also found to be nontoxic to liver cancer cell lines, that is, HepG2 cell lines, as all the

compounds showed activity >300 μM studied through cell viability assay.

3.5 | Molecular docking studies

In silico computational studies have become an integral part of the studies for identifying the targets for diverse ligands due to the non-availability of the resources. Hence, the molecular docking studies of the synthesized compounds in the active site of crystal structure of InhA (pdb: 3FNE) bound to a triclosan derivative was performed. This crystal structure was downloaded from Protein Data Bank, and it consisted of two ligands, that is, triclosan derivative and NAD 300. The protein was corrected structurally stepwise in silico using the protein preparation wizard module of Schrodinger 2017-4. A Glide XP procedure was used. The docking procedure was validated by splitting the prepared protein into ligand and protein. The ligand that is a triclosan derivative was redocked into the same binding site. The observed RMSD score of 0.4163 Å indicated a similar binding pattern of redocked ligand compared with cocrystallized ligand, thereby confirming the accuracy of the experiment. Furthermore, all the ligands and triclosan were docked at the same binding site of protein and the binding mode of the synthesized molecules was compared with triclosan. Also the binding interaction of the molecules with the target protein residue was studied. The compounds showed hydrogen bond interactions with NAD 300 such as triclosan and additional interaction with phenylalanine 149 active site residue. The predicted binding energies of the compounds are listed in Table 3.

The most active compound **2j** (MIC 19 μM) showed a dock score of −9.270 kcal/mol and a binding affinity of −61.84 kcal/mol. The compound exhibited one hydrogen bonding interaction with NAD 300. One π–π stacking interaction was observed between ring B and phenylalanine 149 (Figure 1a).

Compound **2i** (MIC 20.069 μM) displayed a dock score of −9.563 kcal/mol and a binding energy of −71.64 kcal/mol,

TABLE 3 Molecular docking results of compounds (**2a**–**2m**)

Compounds	Docking score (kcal/mol)	Prime MMGBSA dG bind (kcal/mol)	Number of interacting bonds	Interacting residues	Hydrogen bond distance (Å)
2a	−9.066	−66.60	1 H-bond 1 π–π stack	NAD 300 Phenylalanine 149	2.11
2b	−7.025	−63.17	1 H-bond 1 π–π stack	NAD 300 Phenylalanine 149	1.90
2c	−8.798	−62.37	1 H-bond 1 π–π stack	NAD 300	2.29
2d	−8.161	−62.83	1 H-bond 1 π–π stack	NAD 300 Phenylalanine 149	1.92
2e	−8.211	−61.09	1 H-bond 1 π–π stack	NAD 300	1.46
2f	−9.095	−65.43	2 H-bond 1 π–π stack	NAD 300 Tyrosine 158 Phenylalanine 149	2.17
2g	−8.483	−48.91	–	–	–
2h	−8.909	−70.25	1 π–π stack	Phenylalanine 149	–
2i	−9.563	−71.64	1 H-bond 1 π–π stack	NAD 300 Phenylalanine 149	1.84
2j	−9.270	−61.84	1 H-bond 1 π–π stack	NAD 300 Phenylalanine 149	2.17
2k	−9.608	−66.21	1 H-bond 1 π–π stack	NAD 300 Phenylalanine 149	2.13
2l	−7.102	−73.39	1 H-bond 1 π–π stack	NAD 300 Tyrosine 158 Phenylalanine 149	1.96
2m	−9.029	−69.43	1 π–π stack	Phenylalanine 149	–
Triclosan	−8.523	−60.49	2 H-bond 1 π–π stack	NAD 300 Phenylalanine 149	2.47, 1.85

Abbreviations: H, hydrogen; NAD, nicotinamide adenine dinucleotide.

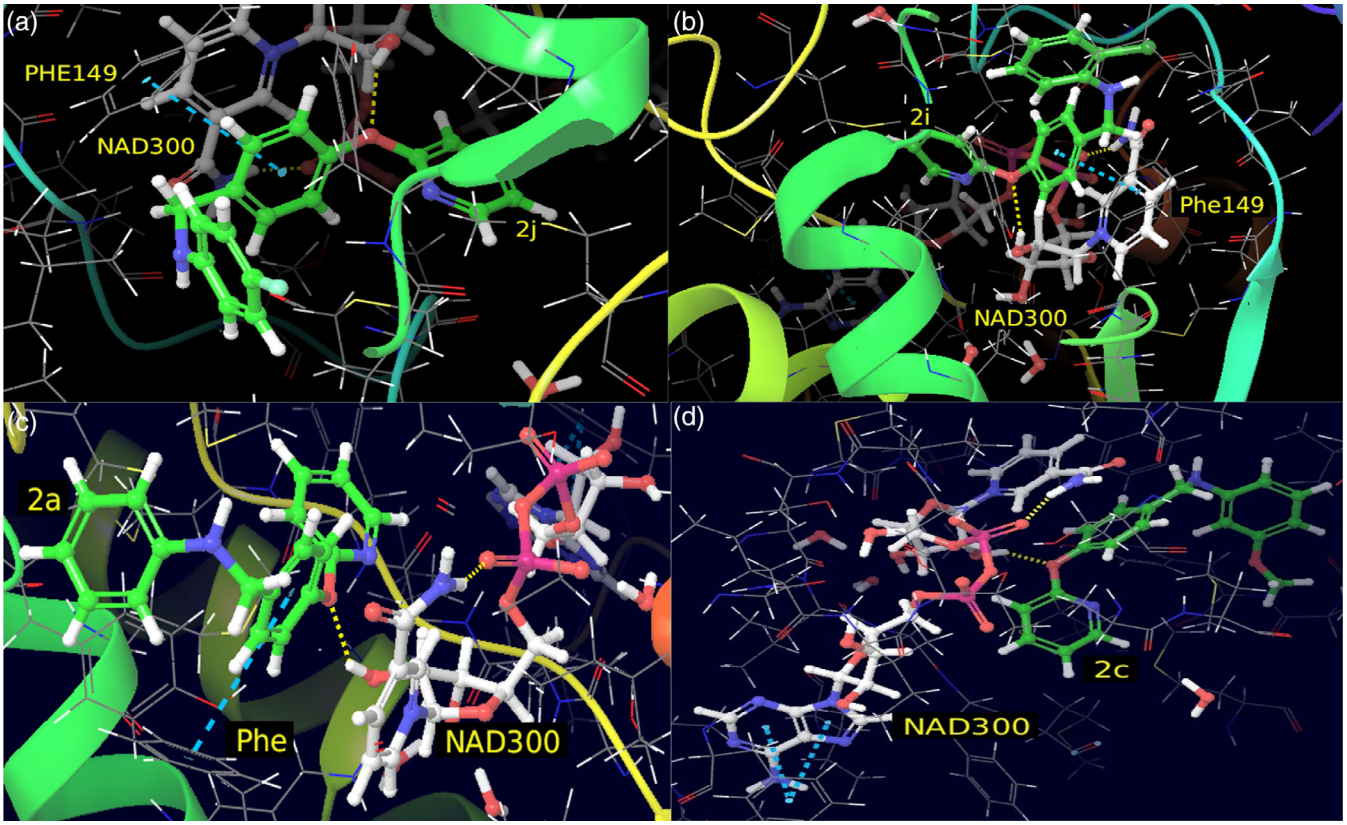

FIGURE 1 (a) Molecular docking interaction of compound **2j** (green) with NAD 300 ligand and phenylalanine 149 residue of Mtb InhA (PDB 3FNE). (b) Molecular docking interaction of compound **2i** (green) with NAD 300 ligand and phenylalanine 149 residue of Mtb InhA (PDB 3FNE). (c) Molecular docking interaction of compound **2a** (green) with NAD 300 ligand and phenylalanine residue of Mtb InhA (PDB 3FNE). (d) Molecular docking interaction of compound **2c** (green) with NAD 300 ligand of MTb Inh A (PDB 3FNE). Phe, phenylalanine
Note. Dotted yellow line shows the hydrogen bonding interaction

respectively. It showed similar hydrogen bonding and π–π stacking interaction as compound **2j** (Figure 1b).**

Compound **2d** (MIC 21.55 μM), **2c** (MIC 25 μM), and **2a** (MIC 25 μM) displayed dock scores of −8.161, −8.978, and − 9.066 kcal/mol individually and binding energies of −62.83, −62.37, and − 66.60 kcal/mol, respectively. Compounds **2d** and **2a** showed hydrogen bonding interactions with NAD 300 and one π–π stacking interaction between B ring and phenylalanine 149. Figure 1c depicts molecular interactions between compound **2a** and the catalytic target residue. Compound **2c** displayed hydrogen-bonding interactions with NAD 300 (Figure 1d).

The molecular docking interactions of the synthesized compounds were compared with triclosan. Triclosan showed a dock score of −8.523 kcal/mol, a binding energy of −60.49 kcal/mol, and two hydrogen-bonding interactions with NAD 300. Figure 2 displays molecular interactions between triclosan and catalytic site residues of protein.

The theoretical predictions through molecular docking studies were found to be in agreement with the experimentally observed antitubercular activity results. The most active compounds were found to have good dock score, high binding affinities, and a greater number of interactions with the protein residues in comparison with triclosan.

3.6 | MD analysis

Compounds **2i-InhA complex** and **triclosan-InhA complex** were subjected to MD simulation. Compound **2i** was selected as it showed potent antitubercular activity for both weeks, that is, 20 μM. The stability of the protein structural model and binding pattern of triclosan and **2i** with InhA enzyme was examined throughout the MD simulations. This was evident through conformational changes occurring in the structure and the interaction between ligand and protein. MD simulation studies were carried out with an explicit solvent for 20 ns. The complex stability during MD simulation was calculated by aligning the protein backbone frames to the backbone of initial frame. The overall deviation from the starting structure was measured by RMSD. Figure 3 depicts that **2i-InhA** is stabilized much better when compared with **triclosan-InhA** during the simulation studies, which is visible through higher structural fluctuations of triclosan than **2i**. The RMSD plot for compound **2i** suggests that the protein backbone RMSD recorded during simulation showed high fluctuations for the initial 5 ns due to the initial protein structural stabilization for the **2i** protein complex. The backbone RMSD observed for protein between 5 to 20 ns was in the range of 2.2 to 1.7 Å, compared with that of the original structure and was within a range of 0.8 Å to 0.6 Å. The ligand **(2i)** RMSD remained within the range of 2.9 to 1.9 Å in comparison

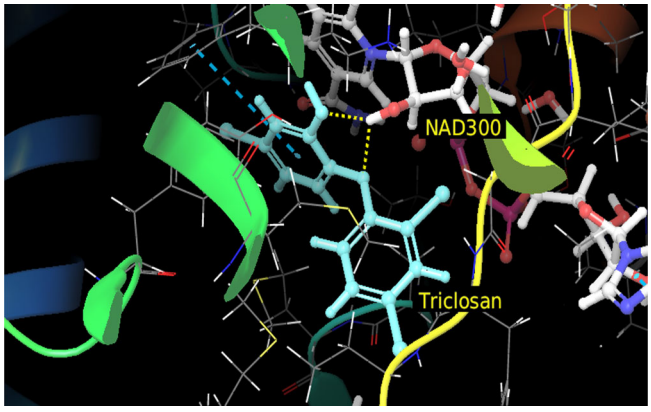

FIGURE 2 Molecular docking interaction of triclosan (blue) with NAD 300 ligand of Mtb InhA (PDB 3FNE).
Note: Dotted yellow line shows the hydrogen bonding interaction

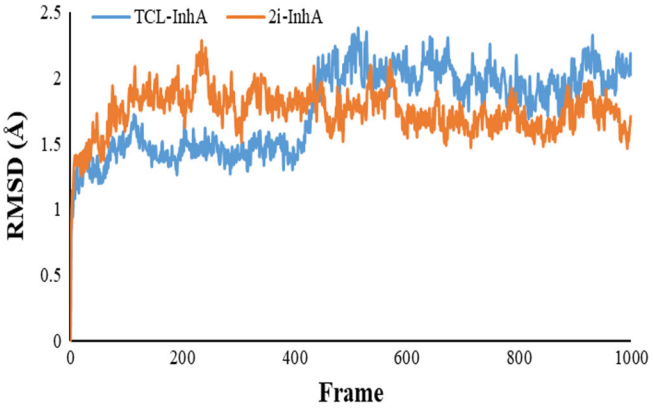

FIGURE 3 The RMSD of protein backbone structure in comparison with the original structure for molecule (a) **2i** and (b) **Triclosan**

with the original structure and was within the range of 1.0 Å to 0.6 Å, suggesting the formation of the stable ligand–protein complex. **Triclosan-InhA complex** stabilized at 11.64 ns comparatively and exhibited slightly higher structural fluctuations during MD simulation. The structural deviations observed for protein between 11 and 20 ns were in the range of 2.3 to 0.72 Å compared with that of the original structure and was within the range of 2.0 Å to 0.7 Å and the triclosan RMSD remained in the range of 1.53 Å to 0.57 Å compared with the original structure. The ligand fluctuations in MD trajectory observed to be slightly higher for triclosan, compared with that of molecule **2i**, depicting that **2i** is stabilizing the complex better than the triclosan.

Root mean square fluctuation (RMSF) values were used to depict the fluctuations of each residue present in protein over the simulation time period (Figure 4). Higher peaks represent the amino acid residues that fluctuate the most. The highest fluctuating residue was observed to be A:Leu 207 with RMSF value of 3.22 Å and A:Ala 252 with RMSF value of 2.71 Å. The high fluctuations also represent maximum binding between the protein and the ligand. RMSF fluctuation for the remaining protein was observed within the range of 0.64 Å to 2.20 Å. For **triclosan-InhA complex**, protein RMSF fluctuation was observed in the range of 1.14–2.3 Å. The most fluctuating amino acid residues were A:Thr 259 and A:Ala 252 with RMSF values of 2.83 Å and 2.82 Å, respectively.

Ligand root mean square fluctuation (L-RMSF) depicts characteristic changes in the ligand atom positions during the simulation time interval (Figure 5). Carbon atoms at B ring of **2i** compound were found to fluctuate the most. The RMSF value was observed within the range of 1.00–2.00 Å. The chloro group at the second position in ring A and the OH group on ring B of triclosan displayed maximum fluctuation with RMSF values of 1.11 and 0.96 Å, respectively.

The nonbonded intermolecular interactions between the InhA-binding residue and the ligand **2i** and **triclosan** observed during the

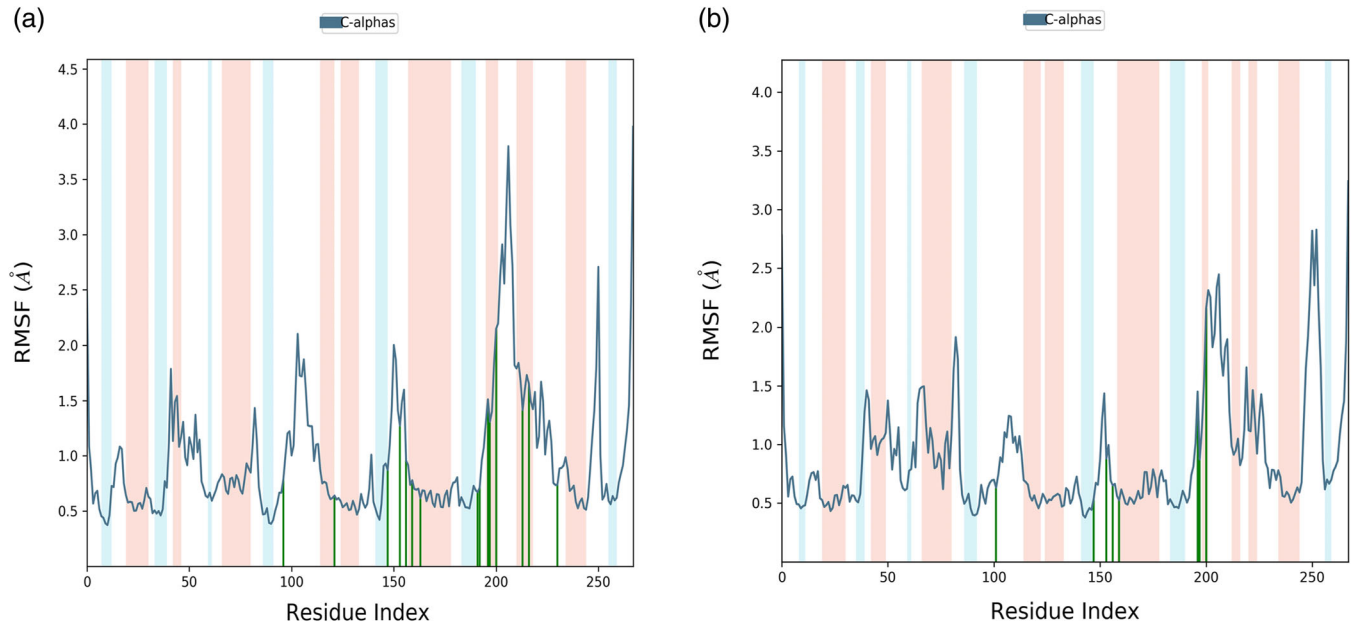

FIGURE 4 Protein RMSF plot during molecular dynamics simulation: (a) **2i-InhA complex**; (b) **Triclosan-InhA complex**

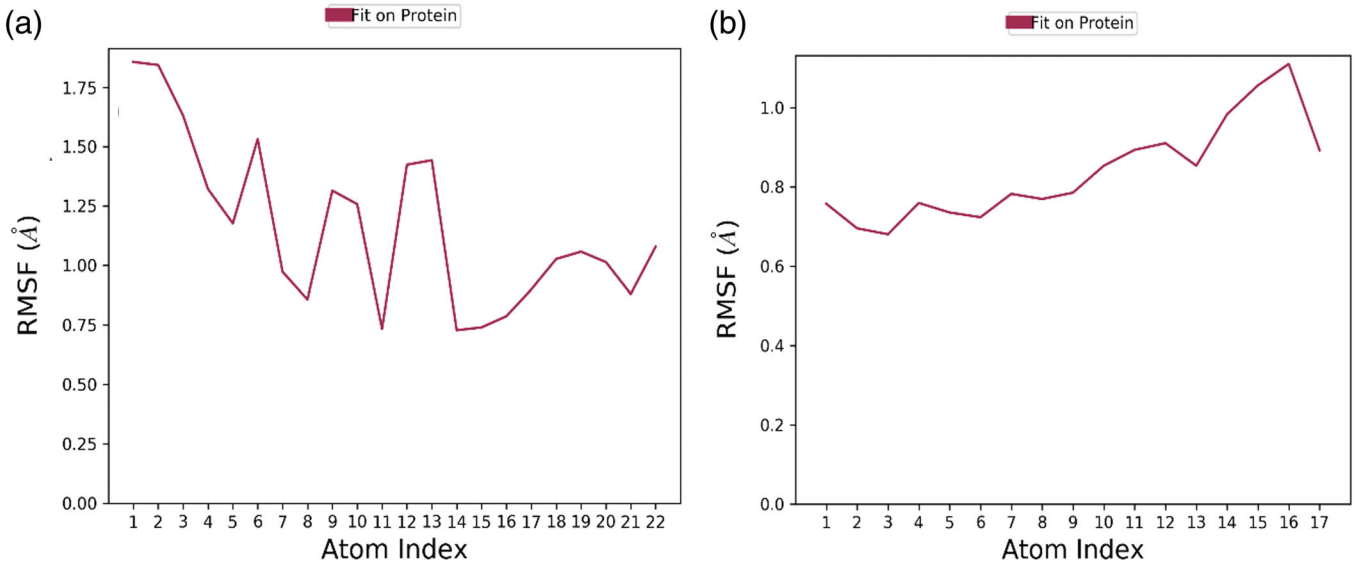

FIGURE 5 Ligand RMSF plot during molecular dynamics simulation: (a) **2i-InhA complex**; (b) **Triclosan-InhA complex**

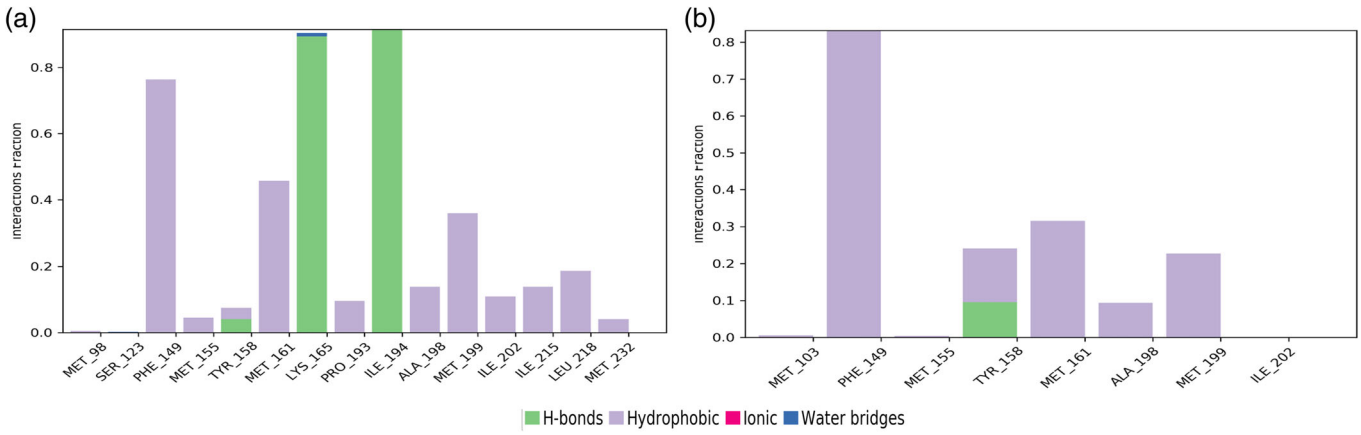

FIGURE 6 Plot of protein interactions with ligand (a) **2i** and (b) **Triclosan** as monitored throughout the simulation

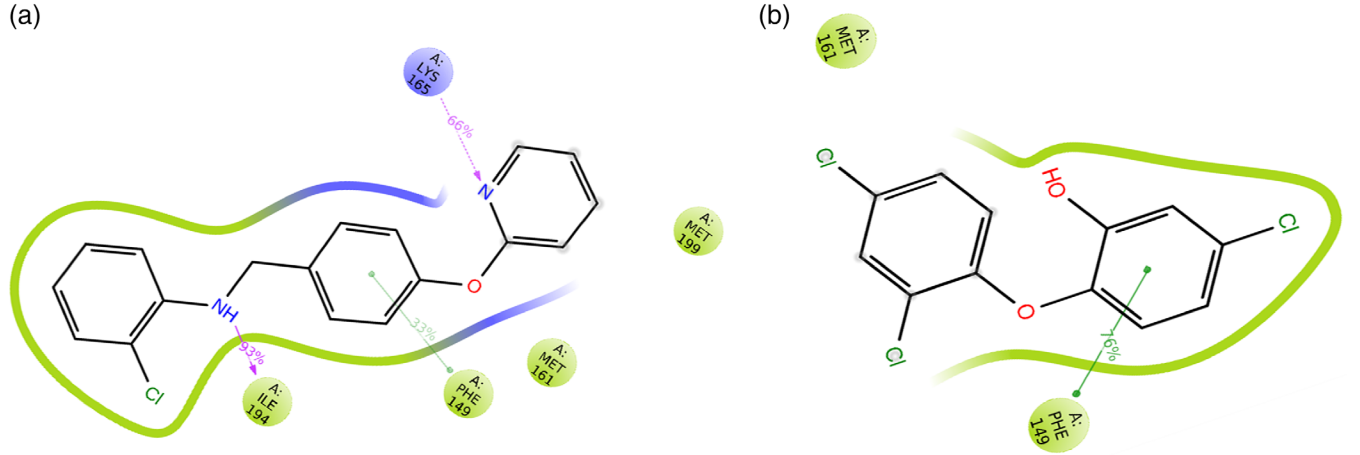

FIGURE 7 The atomic interactions of ligand (a) **2i** and (b) **Triclosan** with the key amino acid residues at the active site

TABLE 4 Predicted ADME properties and drug-likeness properties of the compounds (**2a**–**2m**) as per the QikProp software application

Compounds	QPlogBB[a]	QPPMDCK[b] nm/s	QPlogKhsa[c]	QPlogS[d]	CNS[e]	% HOA[f]	QPlogPo/w[g]	PSA[h]	Lipinskirule of five[i]
2a	−0.093	2,503.828	0.541	−4.972	0	100.0	3.69	30.07	0
2b	0.003	3,733.112	0.582	−5.395	0	100.0	3.79	38.37	0
2c	0.007	3,767.527	0.578	−5.382	0	100.0	3.79	38.36	0
2d	−0.104	2,505.132	0.706	−5.564	1	100.0	4.18	30.07	0
2e	−0.102	2,511.431	0.706	−5.558	1	100.0	4.18	30.07	0
2f	0.114	4,120.574	0.666	−5.279	1	100.0	4.18	28.37	0
2g	0.074	6,169.814	0.662	−5.724	1	100.0	4.7	30.08	0
2h	0.075	6,188.495	0.662	−5.72	1	100.0	4.7	30.09	0
2i	0.085	5,741.128	0.605	−5.209	1	100.0	4.7	28.81	0
2j	0.018	4,520.428	0.585	−5.342	1	100.0	4.13	30.07	0
2k	0.026	4,666.815	0.582	−5.281	1	100.0	4.13	29.5	0
2l	0.086	6,636.604	0.686	−5.841	1	100.0	4.13	30.09	0
2m	0.088	6,658.051	0.687	−5.837	1	100.0	4.8	30.08	0
TCL	0.396	10,000	0.394	−4.52	1	100.0	4.75	28.767	0

[a]Predicted brain/blood partition coefficient (acceptable range: −3.0 to −1.2).
[b]Predicted apparent MDCK cell permeability (acceptable range: <25 poor to >500 great).
[c]Prediction of binding to human serum albumin (acceptable range: −1.5 to 1.5).
[d]Predicted aqueous solubility in mol/L (acceptable range: −6.5 to 0.5).
[e]Predicted central nervous system activity on a −2 (inactive) to +2 (active) scale.
[f]Percentage human oral absorption (<25% is poor and >80% is high).
[g]Log *p* in o/w (acceptable range: −2.0 to 6.5).
[h]Polar surface area (≤140 Å^2).
[i]Lipinski's rule of five: the number of violations to the Lipinski's rule of five.

MD simulation are shown in Figure 6. All the ligand–protein interactions observed in the docking study were present throughout the MD simulation. The molecule **2i** exhibited hydrogen bonding and hydrophobic interactions. The molecule also formed water bridge interaction with lysine 165 amino acid residue. Most prominent hydrogen bonding interaction between target receptor and ligand was observed with A:Lysine 165 with 89.4% occupancy and A:Isoleucine 194 amino acid residues with 91.5% occupancy. The hydrophobic interaction was mostly observed with A:Phenylalanine 149 with 76.3% occupancy. The residues A:Met 155, A-Tyr158 A:Met 161, A:Pro193, A:Ala 198, A:Met 199, A:Ile 215, A:Leu 218, and A:Met 232 also took part in hydrophobic interactions but showed very less occupancy. These interactions during the simulation time period make stable protein–ligand complexes. Triclosan showed hydrogen-bonding interaction with A:Tyr 158 and hydrophobic interaction with A:Phe 149, A:Tyr 158, A: Met 161, A: Ala 198, and A: Met 199. Among these interactions, only phenylalanine 149 occupancy was observed to be 83.0% with triclosan. The other residues displayed occupancy less than 30%. This depicts that during simulation time compound **2i** interacted and maximum interaction occurred with amino acid residues, whereas triclosan interactions were found to be less.

The residues that interacted with ligands for more than 30% of the simulation time in the trajectory are shown as ligand–protein contacts (Figure 7). The residue A:Lys 165 displayed hydrogen-bonding interaction with nitrogen of pyridine ring and A:Ile194 showed hydrogen-bonding interaction with NH group. B ring of the ligand moiety formed π–π interaction with Phe 149. Triclosan displayed π–π stacking interaction with phenylalanine 149 amino acid residue and its B ring.

The interaction observed between protein and **2i** was stronger than the triclosan–protein complex. Owing to this, **2i** is showing a higher potency than triclosan.

3.7 | Lipinski's rule for drug-likeliness and in silico ADME prediction

The synthesized compounds were investigated for physical descriptors as well as pharmaceutically significant properties using the QikProp v 5.4 tool of Schrodinger release 2017-4. The synthesized molecules followed the Lipinski's rule of five as given in Table 4 and showed better partition coefficients than triclosan.

The parameters assessed were hydrogen bond acceptor, hydrogen bond donors, partition coefficient between octanol and water (log *p*) and polar surface area (PSA). In silico ADME prediction is very important for selecting suitable drug candidates, hence these parameters were studied using Schrodinger suite release 2017-4. The in silico ADME properties of the synthesized compounds are given in Table 4.

The predicted values for QPlogBB (which predicts brain/blood partition coefficient for drugs delivered orally) are from −3.0 to 1.2. The QPPMDCK was analyzed to predict the apparent Madin–Darby Canine Kidney (MDCK) cell permeability in nm/s. The permeability of the test compounds to these cells is used to assess ability to permeate

the blood–brain barrier. A value <25 indicates poor permeability and value >500 indicates good permeability. The QPlogKhsa property predicts a given compound's binding affinity to human serum albumin. All the synthesized compounds showed acceptable ADME properties. The predicted aqueous solubility (QPlogS) of the synthesized compounds was found to be above −4.972 mol dm^{-3} in comparison with triclosan (−4.92 mol dm^{-3}). The compounds were found to be inactive for central nervous system (CNS) activity. All the synthesized molecules showed acceptable ADME properties and followed the Lipinski's rule.

4 | CONCLUSION

In conclusion, we have successfully demonstrated the synthesis of a series of 13 *N*-(4-(pyridin-2-yloxy)benzyl)arylamines and tested them for their in vitro antitubercular activity against MTb H37Rv. Most of the compounds exhibited significant antitubercular activity when compared with triclosan and preliminary antibacterial activity, suggesting their activity toward *B. subtilis* and *S. aureus*. The synthesized compounds were found to be safe by in vitro cytotoxicity evaluation. The compounds synthesized exhibited drug-like properties, and ADME properties were found to be within the acceptable range. Supporting in silico studies revealed that their interaction and dock score was better in comparison with the triclosan. Molecular docking studies were followed by an MD simulation study of the active derivative **2i** that showed good fitting, which is in agreement with the in vitro results, hence the synthesized compounds have further scope for structural modifications and explore this moiety as potent antitubercular agents.

ACKNOWLEDGMENTS

The authors thank the Department of Biotechnology, Government of India, for providing the research grant (BT/Bio-CARe/03/10087/2013-14) for financial support and Manipal Academy of Higher Education for providing the facilities to carry out this research work. This work was funded in part by the Intramural Research Program of the NIH, NIAID. The authors also acknowledges the Manipal Schrodinger Centre for Molecular Simulations, Manipal Academy of Higher Education, for providing the facilities for in silico studies.

CONFLICT OF INTEREST

The authors declare no conflict of interest.

ORCID

G. Gautham Shenoy https://orcid.org/0000-0002-1312-6257

REFERENCES

Ajay, A., Singh, V., Singh, S., Pandey, S., Gunjan, S., Dubey, D., … Tripathi, R. (2010). Synthesis and bio-evaluation of alkylaminoaryl phenyl cyclopropyl methanones as antitubercular and antimalarial agents. *Bioorganic Medicinal Chemistry*, *18*(23), 8289–8830.

Ammerman, N. C., Beier-Sexton, M., & Azad, A. F. (2008). Growth and maintenance of Vero cell lines. *Current Protocols in Microbiolgy*. 2008; Appendix 4:Appendix–4E. https://doi.org/10.1002/9780471729259.mca04es11

Bari, B. S., & Haswani, N. G. (2017). Design, synthesis and molecular docking study of thienopyrimidin-4(3H)-thiones as antifungal agents. *Journal of Saudi Chemical Society*, *21*, S264–S274.

Barot, K. P., Jain, S. V., Gupta, N., Kremer, L., Singh, S., Takale, V. B., … Ghate, M. D. (2014). Design, synthesis and docking studies of some novel (R)-2-(4′-chlorophenyl)-3-(4′-nitrophenyl)-1,2,3,5-tetrahydrobenzo [4,5] imidazo [1,2-c] pyrimidin-4-ol derivatives as antitubercular agents. *European Journal of Medicinal Chemistry*, *83*, 245–255.

Barry, C. E., Crick, D. C., & McNeil, M. R. (2007). Targeting the formation of the cell wall core of *M. tuberculosis*. *Infectious Disorders Drug Targets*, *7*(2), 182–202.

Bloch, K. (1977). Control mechanisms for fatty acid synthesis in *Mycobacterium smegmatis*. *Advances in Enzymology and Related Areas of Molecular Biology*, *45*, 1–84.

Desmond Molecular Dynamics System, D. E. Shaw Research, New York, NY, 2015. Maestro-desmond interoperability tools, Schrödinger, New York, NY, 2015.

Ece, A. (2019). Towards more effective acetylcholinesterase inhibitors: A comprehensive modelling study based on human acetylcholinesterase protein–drug complex. *Journal of Biomolecular Structure and Dynamics*. https://doi.org/10.1080/07391102.2019.1583606

Freundlich, J. S., Wang, F., Vilchèze, C., Gulcin Gulten, G., Langley, R., Schiehser, G. A., … Sacchettini, J. C. (2009). Triclosan derivatives: Towards potent inhibitors of drugsensitive and drug-resistant *Mycobacterium tuberculosis*. *ChemMedChem*, *4*(2), 241–248.

Friesner, R. A., Murphy, R. B., Repasky, M. P., Frye, L. L., Greenwood, J. R., Halgren, T. A., … Mainz, D. T. (2006). Extra precision glide: Docking and scoring incorporating a model of hydrophobic enclosure for protein-ligand complexes. *Journal of Medicinal Chemistry*, *49*, 6177–6196.

Gandhi, N. R., Moll, A., Sturm, A. W., Pawinski, R., Govender, T., Lalloo, U., … Friedland, G. (2006). Extensively drug-resistant tuberculosis as a cause of death in patients co-infected with tuberculosis and HIV in a rural area of South Africa. *Lancet*, *368*(9547), 1575–1580.

Guo, S., Song, Y., Huang, Q., Yuan, H., Wan, B., Wang, Y., … Kozikowski, A. P. (2010). Identification, synthesis, and pharmacological evaluation of tetrahydroindazole based ligands as novel antituberculosis agents. *Journal of Medicinal Chemistry*, *53*(2), 649–659.

Harder, E., Damm, W., Maple, J., Wu, C., Reboul, M., Xiang, J. Y., … Friesner, R. A. (2015). OPLS3: A force field providing broad coverage of drug-like small molecules and proteins. *Journal of Chemical Theory and Computation*, *12*(1), 281–296.

Hartkoorn, R. C., Sala, C., Neres, J., Pojer, F., Magnet, S., Mukherjee, R., … Cole, S. T. (2012). Towards a new tuberculosis drug: Pyridomycin—nature's isoniazid. *EMBO Molecular Medicine*, *4*, 1032–1042.

Johnson, R., Streicher, E. M., Louw, G. E., Warren, R. M., van Helden, P. D., & Victor, T. C. (2006). Drug resistance in *Mycobacterium tuberculosis*. *Current Issues in Molecular Biology*, *8*(2), 97–111.

Kaniga, K., Cirillo, D. M., Hoffner, S., Ismail, N. A., Kaur, D., Lounis, N., … Venter, A. (2016). A multilaboratory, multicountry study to determine MIC quality control ranges for phenotypic drug susceptibility testing of selected first-line antituberculosis drugs, second-line injectables, fluoroquinolones, clofazimine, and linezolid. 54 (12). *Journal of Clinical Microbiology*, *54*(12), 2963–2968.

Levy, C. W., Roujeinikova, A., Sedelnikova, S., Baker, P. J., Stuitje, A. R., Slabas, A. R., … Rafferty, J. B. (1999). Molecular basis of triclosan activity. *Nature*, *398*(6726), 383–384.

Lipinski, C. A., Lombardo, F., Dominy, B. W., & Feeney, P. J. (1997). Experimental and computational approaches to estimate solubility and permeability in drug discovery and development settings. *Advanced Drug Delivery Reviews*., *46*(1–3), 3–26.

Lu, H., & Tonge, P. J. (2008). Inhibitors of FabI, an enzyme drug target in the bacterial fatty acid biosynthesis pathway. *Accounts of Chemical Research*., *41*(1), 11–20.

Malikanti, R., Vadija, R., Veeravarapu, H., Mustyala, K. K., Malkhed, V., & Vuruputuri, U. (2017). Identification of small molecular ligands as potent inhibitors of fatty acid metabolism in *Mycobacterium tuberculosis*. *Journal of Molecular Structure*, *1150*, 227–241.

McLeod, R., Muench, S. P., Rafferty, J. B., Kyle, D. E., Mui, E. J., Kirisits, M. J., … Rice, D. W. (2001). Triclosan inhibits the growth of plasmodium falciparum and toxoplasma gondii by inhibition of apicomplexan fab I. *International Journal for Parasitology*, *31*(2), 109–113.

Migliori, G. B., De Iaco, G., Besozzi, G., Centis, R., & Cirillo, D. M. (2007). First tuberculosis cases in Italy resistant to all tested drugs. *Euro Surveillance*, *12*, E070517.1.

Nguyen, M., Claparols, C., Bernadou, J., & Meunier, B. (2001). A fast and efficient metal-mediated oxidation of isoniazid and identification of isoniazid–NAD (H) adducts. *Chembiochem*, *2*(12), 877–883.

Rozwarski, D. A., Grant, G. A., Barton, D. H., Jacobs, W. R., & Sacchettini, J. C. (1998). Modification of the NADH of the isoniazid target (InhA) from *Mycobacterium tuberculosis*. *Science*, *279*(5347), 98–102.

Schiff base formation (2014). Chemistrylibretexts. https://chem.libretexts.org/Bookshelves/Organic_Chemistry/Book%3A_Organic_Chemistry_with_a_Biological_Emphasis_(Soderberg)/11%3A_Nucleophilic_carbonyl_addition_reactions/11.6%3A_Imine_(Schiff_base)_formation. Accessed June 20, 2018.

Schrödinger Release 2017-4: Glide module version 77011, Schrödinger, LLC, New York, NY, 2017.

Sharma, A., Gudala, S., Ambati, S. R., Penta, S., Bomma, Y., Janapala, V. R., … Kumar, A. (2018). Synthesis, anticancer evaluation and molecular docking studies of novel (4-hydroxy 2-thioxo-3,4-dihydro-2H-[1,3]thiazin-6-yl)-chromen-2-ones via a multicomponent approach. *Journal of Chinese Chemical Society*, *65*, 810–821. https://doi.org/10.1002/jccs.201700340

Sharma, R., Kothapalli, R., Dongen, A. M. J. V., & Swaminathan, K. (2012). Chemoinformatic identification of novel inhibitors against *Mycobacterium tuberculosis* L-aspartate adecarboxylase. *PLoS One*, *7*(3), e33521.

Soares de Melo, C., Feng, T. S., van der Westhuyzen, R., Gessner, R. K., Street, L. J., Morgans, G. L., … Chibale, K. (2015). Aminopyrazolo[1,5-a]pyrimidines as potential inhibitors of *Mycobacterium tuberculosis*: Structure activity relationships and ADME characterization. *Bioorganic Medicinal Chemistry*, *23*(22), 7240–7250.

Taft, C. A., da Silva, V. B., & da Silva, C. H. T. P. (2008). Current topics in computer-aided drug design. *Journal of Pharmaceutical Sciences*, *97*(3), 1089–1098.

Tahtaci, H., Karacık, H., Ece, A., Er, M., & Seker, M. G. (2018). Design, Synthesis, SAR and Molecular Modeling Studies of Novel Imidazo[2,1-b][1,3,4]Thiadiazole Derivatives as Highly Potent Antimicrobial Agents. *Molecular Informatics*, *37(3)*, 1700083.

Thomas, A. C., Kar, S. S., Bairy, I., Bhat, G. V., Shenoy, P. V., & Gautham, G. S. (2015). Design, synthesis and evaluation of antitubercular activity of triclosan analogues. *Arabian Journal of Chemistry*. https://doi.org/10.1016/j.arabjc.2015.09.003

Udwadia, Z. F., Amale, R. A., Ajbani, K. K., & Rodrigues, C. (2012). Totally drug-resistant tuberculosis in India. *Clinical Infectious Diseases*, *54*(4), 579–581.

Veber, D. F., Johnson, S. R., Cheng, H. Y., Smith, B. R., Ward, K. W., & Kopple, K. D. (2002). Molecular properties that influence the oral bioavailability of drug candidates. *Journal of Medicinal Chemistry*, *45*, 2615–2623.

Velayati, A. A., Masjedi, M. R., Farnia, P., Tabarsi, P., Ghanavi, J., ZiaZarifi, A. H., & Hoffner, S. E. (2009). Emergence of new forms of totally drug-resistant tuberculosis bacillis uper extensively drug-resistant tuberculosis or totally drug-resistant strains in Iran. *Chest*, *136*(2), 420–425.

Vilchèze, C., & Jacobs, W. R. (2014). Resistance to isoniazid and ethionamide in *Mycobacterium tuberculosis*: Genes, mutations, and causalities. *Microbiology Spectrum*, *2*(4), MGM2-0014-2013.

W. H.O, *Global tuberculosis report* 2018.

Wang, L. Q., Falany, C. N., & James, M. O. (2004). Triclosan as a substrate and inhibitor of 3′-phosphoadenosine 5′-phosphosulfate-sulfotransferase and UDP-glucuronosyl transferase in human liver fractions. *Drug Metabolism and Disposition*, *32*(10), 1162–1169.

Zhang, Y., Heym, B., Allen, B., Young, D., & Cole, S. (1992). The catalase-peroxidase gene and isoniazid resistance of *Mycobacterium tuberculosis*. *Nature*, *358*(6387), 591–593.

Zhao, X., Yu, H., Yu, S., Wang, F., Sacchettini, J. C., & Magliozzo, R. S. (2006). Hydrogen peroxide-mediated isoniazid activation catalyzed by *Mycobacterium tuberculosis* catalase-peroxidase (KatG) and its S315T mutant. *Biochemistry*, *45*(13), 4131–4140.

Zheng, S., Kaur, G., Wang, H., Li, M., Macnaughtan, M., Yang, X., … Ke, H. (2018). Design, synthesis, and structure–activity relationship, molecular modeling, and NMR studies of a series of phenyl alkyl ketones as highly potent and selective phosphodiesterase-4 inhibitors. *Journal of Medicinal Chemistry*, *51*(24), 7673–7688.

SUPPORTING INFORMATION

Additional supporting information may be found online in the Supporting Information section at the end of this article.

How to cite this article: Verma R, Boshoff HIM, Arora K, et al. Synthesis, evaluation, molecular docking, and molecular dynamics studies of novel *N*-(4-[pyridin-2-yloxy]benzyl) arylamine derivatives as potential antitubercular agents. *Drug Dev Res*. 2019;1–14. https://doi.org/10.1002/ddr.21623